

Alma Mater Studiorum Università di Bologna  
Archivio istituzionale della ricerca

Ultrafast Spectroscopy: State of the Art and Open Challenges

This is the final peer-reviewed author's accepted manuscript (postprint) of the following publication:

*Published Version:*

Maiuri M., Garavelli M., Cerullo G. (2020). Ultrafast Spectroscopy: State of the Art and Open Challenges. JOURNAL OF THE AMERICAN CHEMICAL SOCIETY, 142(1), 3-15 [10.1021/jacs.9b10533].

*Availability:*

This version is available at: <https://hdl.handle.net/11585/785792> since: 2020-12-28

*Published:*

DOI: <http://doi.org/10.1021/jacs.9b10533>

*Terms of use:*

Some rights reserved. The terms and conditions for the reuse of this version of the manuscript are specified in the publishing policy. For all terms of use and more information see the publisher's website.

This item was downloaded from IRIS Università di Bologna (<https://cris.unibo.it/>).  
When citing, please refer to the published version.

(Article begins on next page)

This is the final peer-reviewed accepted manuscript of:

**Margherita Maiuri, Marco Garavelli and Giulio Cerullo “Ultrafast spectroscopy: state of the art and open challenges” in Journal of the American Chemical Society, 142 (2020), 3-15**

The final published version is available online at:  
<https://dx.doi.org/10.1021/jacs.9b10533>

#### Terms of use:

Some rights reserved. The terms and conditions for the reuse of this version of the manuscript are specified in the publishing policy. For all terms of use and more information see the publisher's website.

*This item was downloaded from IRIS Università di Bologna (<https://cris.unibo.it/>)*

***When citing, please refer to the published version.***

# Ultrafast spectroscopy: state of the art and open challenges

Margherita Maiuri<sup>†</sup>, Marco Garavelli<sup>‡</sup> and Giulio Cerullo<sup>\*†</sup>.

<sup>†</sup> IFN-CNR, Dipartimento di Fisica, Politecnico di Milano, Piazza Leonardo da Vinci 32, I-20133 Milano, Italy

<sup>‡</sup> Dipartimento di Chimica Industriale, Università degli Studi di Bologna, Viale del Risorgimento 4, I-40136 Bologna, Italy

---

**ABSTRACT:** Ultrafast spectroscopy techniques use sequences of ultra-short light pulses (with femto- to attosecond durations) to study photoinduced dynamical processes in atoms, molecules, nanostructures and solids. This field of research has experienced an impetuous growth in recent years, due to the technological progress in the generation of ultra-short light pulses and to the development of sophisticated spectroscopic techniques, which greatly increase the amount of information on the process under study. This paper aims at providing a non-exhaustive overview of the state of the art of the field and at pointing out future challenges. We first review the progress in ultrafast optics, which has enabled the generation of broadly tunable light pulses with duration down to a few optical cycles; then we discuss the pump-probe technique, showing examples of its capability to combine very high time resolution, down to the attosecond regime, with broad spectral coverage; we introduce two-dimensional electronic spectroscopy and present results that demonstrate the additional information content provided by the combination of temporal and spectral resolution; we review the achievements of ultrafast X-ray and electron diffraction, which provide time-dependent structural information on photochemical processes; we conclude with a critical analysis of the future open challenges in the field.

---

## INTRODUCTION

The progress of science is intimately linked with the development of tools capable of overcoming the limitations of our senses in the investigation of natural phenomena. In the time domain, visual perception can resolve processes taking places over timescales longer than  $50 \times 10^{-3}$  s. In order to observe in real time faster dynamical processes, one needs to use short illumination times in order to “freeze” the motion of the object under study, allowing taking snapshots of its different evolution phases. The birth of time-resolved optical science is generally ascribed to the high-speed photography experiments performed by Eadweard Muybridge in 1878. Using multiple cameras equipped with fast shutters, allowing exposure times of the order of  $10^{-3}$  s, Muybridge managed to capture different phases of the motion of a horse on the Palo Alto racetrack, shooting a slow-motion movie of the galloping phase and resolving the instant when all four hooves are lifted from the ground.

Following this milestone result, progress in the time resolution of high-speed photography was related to technical achievements in the generation of shorter and shorter light flashes. Stroboscopic photography, introduced by Harold E. Edgerton in the mid XX<sup>th</sup> century<sup>(1)</sup>, brought the time resolution down to the microsecond range. Short light pulses can be used not only to monitor, but also to initiate a dynamical process. The “pump-probe” technique, pioneered by Abraham and Lemoine in 1899<sup>(2)</sup>, employs two synchronized light pulses, the excitation or “pump” pulse which triggers a photoinduced phenomenon, and a delayed “probe” pulse which measures a time-dependent variation of an optical property of the sample, such as absorption or reflection. In 1949, Norrish and Porter<sup>(3)</sup> used a variant of the technique, known as flash photolysis, which combines two electronically delayed light flashes with milli- to microsecond duration, in order to measure long-lived transient intermediates of photochemical reactions, as e.g. aromatic free radicals and triplet states. For their work, they received the Nobel Prize in Chemistry in 1967.

To estimate the time resolution required to follow a molecular process in real time, one can borrow the argument used by Ahmed Zewail in his 1999 Nobel Prize lecture on the development of femtochemistry<sup>(4)</sup>. Considering a typical interatomic distance  $d = 1 \text{ \AA}$  ( $10^{-10}$  m) and an average speed of motion of the atoms  $v = 10^3$  m/s, one readily obtains that a time resolution  $\Delta t = 10^{-13}$  s or better is required to visualize atomic dynamics. This timescale matches the periods of molecular vibrations, which, for frequencies in the  $300\text{--}3000 \text{ cm}^{-1}$  interval, range from  $\approx 100$  to  $\approx 10$  fs. While femtosecond light pulses are able to track atomic motions within molecules, much shorter light pulses are required to follow electronic dynamics within atoms<sup>(5)</sup>. We can obtain a back-of-the-envelope evaluation of the involved timescales by considering the Bohr model of the hydrogen atom. For the  $n = 1$  energy level the orbital period is  $150 \times 10^{-18}$  s, highlighting the need of attosecond ( $1 \text{ as} = 10^{-18}$  s) pulses to resolve electronic dynamics.

Ultrafast optical spectroscopy refers to the ensemble of experimental techniques which use sequences of ultra-short light pulses (with femto- to attosecond durations) to study photoinduced dynamical processes in atoms, molecules, nanostructures and solids. This field of research has experienced an impetuous growth in the last decades, due to: (i) the technological progress in the generation of ultra-short light pulses, in terms of their duration, frequency tunability and stability/reliability; (ii) the development of sophisticated spectroscopy techniques, going beyond the classical pump-probe, enabling to increase the amount of information on the processes under study.

This paper aims at discussing some of the most recent developments and results in the field of ultrafast spectroscopy and at pointing out future challenges and opportunities. It does not have the ambition to provide a comprehensive review, which would necessarily require a much longer article (see e.g. the collection of articles in the Chemical Reviews special issue on Ultrafast Processes in Chemistry<sup>(6)</sup>); rather, its goal is to highlight key recent advances and discuss technological/conceptual bottlenecks. The paper is organized as follows: we first present

the state of the art of ultrashort light pulse generation, which is intimately linked to a deep understanding of light-matter interaction in the nonlinear regime; then we discuss the pump-probe technique, showing examples of its capability to combine very high time resolution (down to the attosecond regime) with broad spectral coverage (from the visible to the soft X-ray range); we introduce two-dimensional (2D) spectroscopy and present results that demonstrate its additional information content; we review the achievements of ultrafast X-ray and electron diffraction, which provide time-dependent structural information on photochemical processes; we conclude with a critical analysis of the current limitations and future challenges of ultrafast optical spectroscopy.

## ULTRASHORT PULSE GENERATION

The field of ultrashort light pulse generation is closely connected to the development of ultrafast laser technology, which has nowadays reached a high level of technical maturity. The starting point of any ultrafast laser system is a mode-locked oscillator including a nonlinear loss mechanism (saturable absorber) and intracavity group velocity dispersion control<sup>(7)</sup>. Oscillators typically generate pulses with nJ-level energy, which is too low for many applications. Pulse energy can be up-scaled by many orders of magnitude using the chirped pulse amplification (CPA) technique<sup>(8),(9)</sup>, where the pulses are first temporally stretched, then amplified and finally recompressed to Fourier-transform-limited duration. CPA allows one to reach very high peak powers and trigger a variety of nonlinear optical processes.

The two main primary sources of ultrashort pulses available today are Ti:sapphire lasers<sup>(9)</sup> and Yb-doped crystal or fiber lasers<sup>(10)</sup>. Ti:sapphire works around 800 nm and provides short pulses, with duration down to 10-20 fs; Yb-based lasers emit around 1040 nm with longer pulsewidths (typically  $\approx 200$  fs) but better potential for scaling both average power and repetition rate. These primary sources are powerful, stable and reliable but operate at fixed wavelengths, with limited tuning capabilities. However, they can pump secondary sources, which exploit nonlinear optical effects to change the frequency, broaden the bandwidth and shorten the duration of the output pulses. Third-order nonlinear effects such as self-phase-modulation<sup>(11)</sup> and white light continuum generation<sup>(12)</sup> are used to broaden the pulse spectrum and generate new frequencies. The second-order nonlinear effect known as optical parametric amplification<sup>(13)</sup> allows the generation of broadly tunable pulses, with duration potentially much shorter than that of the driving pulses<sup>(14)</sup>. Second-harmonic generation and sum-frequency generation enable extension to the ultraviolet, while difference-frequency generation<sup>(15)</sup> and optical rectification<sup>(16)</sup> allow the generation of mid-infrared and THz pulses, respectively.

In summary, secondary sources driven by Ti:sapphire or Yb lasers allow the reliable generation of stable and intense femtosecond light pulses, broadly tunable from the mid-infrared to the ultraviolet range, making ultrafast optical spectroscopy available to a variety of non-specialist users in physics, chemistry and biology<sup>(17)</sup>. The temporal profile of such pulses can be precisely characterized by sophisticated nonlinear optical techniques<sup>(18)</sup>. Table 1 summarizes the main parameters of primary and secondary sources of ultrashort pulses, in terms of wavelength, duration, energy and repetition rate.

Source	Wavelength	Pulse width	Pulse Energy	Repetition rate
<b>Primary solid-state laser sources</b>				
CPA Ti:sapphire	800 nm	5-20 fs	1-10 mJ	1 Hz-200 kHz
CPA Yb laser	1030 nm	150-300 fs	10 $\mu$ J – 1 mJ	1 kHz-10 MHz
<b>Secondary sources by nonlinear frequency conversion</b>				
Ti:sapphire-pumped OPA	450-3000 nm	5-100 fs	1 $\mu$ J-1 mJ	1-200 kHz
Yb-pumped OPA	390-3000 nm	5-200 fs	1-100 $\mu$ J	1 kHz-10 MHz
SHG, SFG	200-400 nm	10-200 fs	0.1-1 $\mu$ J	1-200 kHz
DFG	3-15 $\mu$ m	30-200 fs	0.1-10 $\mu$ J	1-200 kHz
THz	150-600 $\mu$ m	1 ps	0.1 nJ-1 $\mu$ J	1 kHz-100 MHz

Table 1: overview of the performances (wavelength tuning range, pulse width, pulse energy, repetition rate) of primary and secondary sources of ultrashort pulses. OPA: optical parametric amplifier; SHG: second harmonic generation; SFG: sum-frequency generation; DFG: difference frequency generation. The reported parameters reflect the typical performances of the sources commonly found in ultrafast spectroscopy laboratories, and should not be regarded as record performance values.

Ultrashort pulses with much shorter wavelength, down to a few nanometers (corresponding to hundreds of eV photon energy) can be obtained by high-harmonic generation (HHG) from noble gas atoms. In HHG an electron is first tunnel ionized from an atom, then accelerated by the light field and finally recollided with the parent ion, generating by *bremsstrahlung* coherent XUV radiation<sup>(19)</sup>. If the HHG process is confined to a

single recollision event per driving pulse, then a burst of XUV radiation with sub-femtosecond duration is generated<sup>(20)</sup>. Attosecond light pulses (with the current record set at 53 as<sup>(21)</sup>) are now starting to be employed in time-resolved spectroscopy in order to provide direct access to the electronic dynamics in molecules.

Ultrashort pulses with even higher photon energies up to the hard X-rays<sup>(22)</sup> provide access to time-dependent structural dynamics. Femtosecond incoherent hard X-rays are generated from laser-induced plasmas by a mechanism similar to HHG: electrons are first extracted from a metal target by the light field, then accelerated in vacuum and finally recollided with the target, generating X-rays via collisional inner-shell ionization followed by radiative transition of an outer shell electron into the unoccupied inner shell<sup>(23)</sup>. Pioneering experiments with moving metal wires were limited to repetition rates of tens of Hz; use of metal tape targets and optimization of the excitation and collection geometries allowed the generation of high flux hard X-rays at repetition rates up to 1 kHz with negligible timing jitter with respect to the optical driving pulses<sup>(24),(25)</sup>.

Ultrashort X-ray pulses can also be generated from X-ray free electron lasers (XFELs)<sup>(26)</sup>. In an XFEL an electron bunch emitted by a photocathode is accelerated to relativistic energies (up to 10 GeV) by a linear accelerator (with length up to several kms) and then sent to an array of periodically alternating magnetic dipoles, known as undulator. XFELs work in the so-called self-amplified spontaneous emission (SASE) regime<sup>(27)</sup>, where electrons in the bunch interact with spontaneous radiation from the undulator losing or gaining energy, thus forming microbunches spatially separated by the XFEL emission wavelength which all radiate in phase, resulting in coherent emission at a wavelength which is related to the undulator period. SASE XFELs generate intense coherent light pulses with photon energies up to several keVs, reaching the hard X-ray range with femtosecond - and potentially sub-femtosecond - duration. Although several problems related to the energy stability and absolute timing of the pulses still have to be solved, XFELs are demonstrating their power in ultrafast spectroscopy, by allowing core level spectroscopy in atoms and ultrafast X-ray diffraction from molecules and solids<sup>(28),(29)</sup>.

Alternatively, ultrashort X-ray pulses can be generated by the so-called synchrotron slicing technique<sup>(30),(31)</sup>, where an ultrashort (50-100 fs) laser pulses is collinearly overlapped and temporally synchronized with the  $\approx 30$ -ps electron bunch of a synchrotron storage ring within an undulator tuned to emit at the laser wavelength. Energy exchange between the light pulse and the electron bunch allows one to energy modulate a short temporal slice of the electron bunch, which is then spatially separated from the main bunch exploiting the dispersion of the electron optical system and used to generate ultrashort X-ray radiation.

It is also possible to replace the optical probe pulse by a pulse of energetic electrons, with De Broglie wavelength short enough to be comparable with interatomic distances in molecules. Femtosecond electron sources, obtained from electron guns illuminated by ultrashort light pulses, face an intrinsic development challenge, due to the natural tendency of the electrons to Coulomb repel each other, broadening their temporal profile. Nevertheless, several techniques for the control of pulse duration at the target have been developed. One simple strategy consists in reducing the distance between source and target, thus minimizing pulse broadening due to propagation<sup>(32)</sup>; another solution exploits the linear energy chirp acquired by the electrons during propagation and makes use of suitable dispersive cavities for electrons, such as radio-frequency cavities, to compress the electron pulse on target<sup>(33)</sup>. Ultrashort electron pulses are currently being used for ultrafast electron diffraction and microscopy<sup>(34),(35)</sup>.

## PUMP-PROBE SPECTROSCOPY

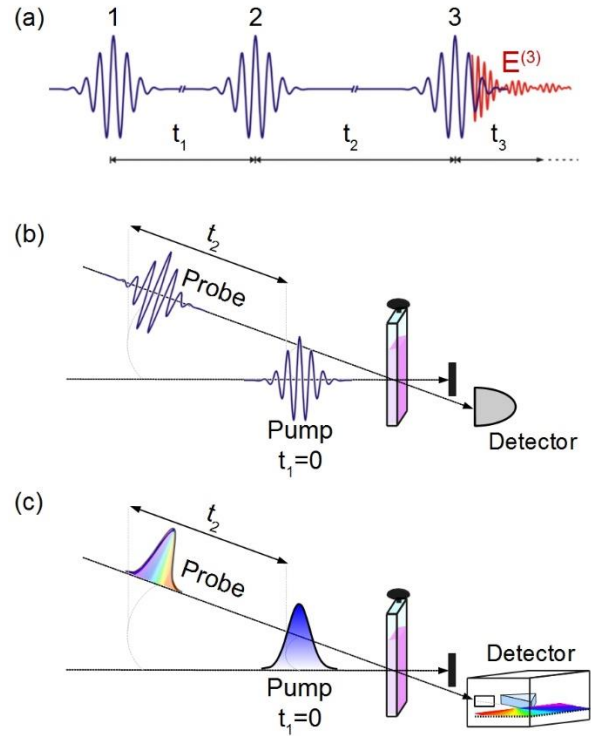


Figure 1. (a) generic scheme of a third-order time-resolved nonlinear optical experiment. (b) pulse sequence in a pump-probe experiment. (c) pump-probe with broadband detection.

Ultrafast spectroscopy experiments typically monitor the third-order nonlinear optical response of the system interacting with a sequence of light pulses. In the most general case, the system is illuminated by three synchronized and time-delayed pulses (see Fig. 1a)<sup>(36)</sup>. Interaction with the electric field of pulse 1 creates a polarization (i.e. a macroscopic coherent superposition of oscillating dipoles) in the sample; interaction with pulse 2, delayed by a time  $t_1$  known as coherence time, changes the population of the sample; finally, interaction with pulse 3, delayed by a time  $t_2$  known as population or waiting time, generates a third order polarization  $P^{(3)}(t_1, t_2, t_3)$ , which in turn irradiates a light field,  $E^{(3)}(t_1, t_2, t_3)$ , proportional to the nonlinear polarization.

In the pump-probe technique, also known as transient absorption (TA), the first two interactions occur with the same pulse (the pump pulse), so that  $t_1 = 0$ . The third pulse (the probe) is non-collinear with the pump and generates the nonlinear field, which is emitted in the same direction as the probe pulse (see Fig. 1b). Systematically varying the delay  $t_2$  between pump and probe pulses by an optical delay line enables one to follow the population dynamics of the system under study in real time. Typically, the pump pulse is periodically switched on and off and the differential absorption ( $\Delta A$ ) of the sample is measured. By using high frequency pump modulation and synchronous detection, one can average out pulse energy fluctuations and achieve high sensitivity, down to the shot noise limit<sup>(37)</sup>. Ideally, in a TA system the pump pulse should be tunable, in order to be able to resonantly excite different transitions, while the probe pulse should be as broadband as possible, in order to access different transitions and extract the maximum amount of infor-

mation on system dynamics. Often, after the sample, the broadband probe pulse is frequency dispersed and its spectrum is recorded with an array of detectors, measuring the delay-dependent differential absorption spectrum  $\Delta A(\omega_3, t_2)$ , where  $\omega_3$  is the probe frequency<sup>(38), (39)</sup> (Figure 1c). Broadband detection allows one to achieve high resolution in the probe frequency, with the temporal resolution determined by the duration of the pump pulse<sup>(40), (41)</sup>.

Although conceptually simple, TA spectroscopy is very powerful due to its versatility and applicability over a wide range of frequencies, from THz to X rays. TA has provided an enormous amount of information on photoinduced dynamical processes in (bio)-molecules<sup>(42)-(44)</sup>, nanostructures<sup>(45), (46)</sup> and solids<sup>(47), (48)</sup>. In the following, we provide two recent examples of its application in which the probing window is extended to the XUV spectral range and the time resolution is pushed to the attosecond domain.

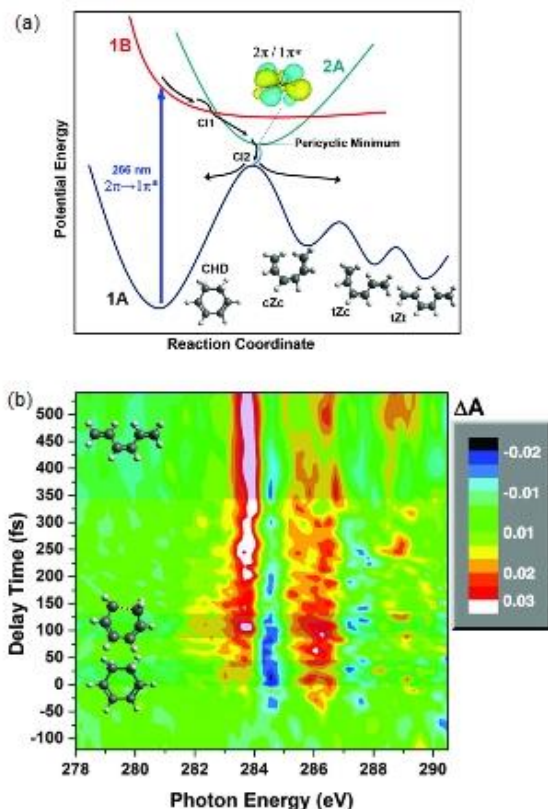


Figure 2. (a) Schematic representation of the relevant PES along the ring-opening reaction coordinate of CHD. Three conformational isomers of the HT photoproduct are formed in the reaction: s-cis, Z,s-cis (cZc), s-trans,Z,s-cis (tZc), and s-trans,Z,s-trans (tZt). (b) A 2D map showing the change in the x-ray absorption ( $\Delta A$ ) as a function of photon energy and of delay between the UV pump and the XUV probe. Figure adapted from Ref. (49).

The first example highlights the ability of HHG, used as a probe, to extend TA spectroscopy to the XUV region, accessing transitions from inner shell core orbitals to valence states and enabling to probe the evolution of the valence electronic structure of a molecule during a photoinduced process. Attar and coworkers<sup>(49)</sup> studied the photoinduced ring-opening reaction of 1,3-cyclohexadiene (CHD), which is a prototypical pericyclic reaction, of crucial importance for the development of the Woodward-Hoffmann stereochemical rules<sup>(50)</sup>. Figure 2a shows

a schematic representation of the potential energy surfaces (PES) of the different states involved in the reaction. UV photoexcitation brings the molecule from the ground state (1A) to the bright excited state (2B) by promoting an electron from the  $2\pi$  to the  $1\pi^*$  molecular orbital. From the Franck-Condon region the wave packet evolves through a first conical intersection (CI) to a dark excited state (2A, of the same symmetry as the ground state)<sup>(51)</sup>. In the dark state, the wave packet reaches the so-called pericyclic minimum and returns to the ground state through a second CI, from which it bifurcates either back to the ground state of the reactant or to the 1,3,5-hexatriene (HT) photoproduct. In the pericyclic minimum, the  $2\pi$  and  $1\pi^*$  molecular orbitals are energetically overlapped and strongly mixed.

The photoinduced ring-opening of gas-phase CHD is initiated with a 4.8 eV pulse in the UV and probed with an XUV pulse produced by HHG and spanning the 275-310 eV region; the temporal resolution of the experiment is  $\approx 120$  fs. The XUV probe covers the near-edge x-ray absorption fine structure (NEXAFS) region around the carbon K edge at 284 eV. NEXAFS probes, from the perspective of the reporter atom, transitions between core levels and empty valence states. When the electronic structure is perturbed by a photoinduced process, time-resolved NEXAFS allows one to follow the time-evolving electronic structure with elemental specificity. Figure 2b reports a map of the  $\Delta A$  signal as a function of probe photon energy and pump-probe delay around the carbon K edge. One can clearly recognize three different phases of the dynamics, associated with characteristic TA spectra representing, respectively, the bright excited state of the CHD reactant, the intermediate dark state and the HT photoproduct. The experimental data are accurately reproduced by non-adiabatic molecular dynamics simulations coupled to time-dependent density functional theory to calculate the NEXAFS spectra.

The dynamics among these states can be clocked by  $\Delta A$  time traces at three specific photon energies in the NEXAFS spectrum, shown in Fig. 3: 284.5 eV (panel a), corresponding to the transition from the carbon 1s core level to the  $1\pi^*$  orbital of the CHD reactant; 284.2 eV (panel c), corresponding to the  $1s \rightarrow 1\pi^*$  transition of the ring-opened HT photoproduct; and 282.2 eV (panel b), corresponding to the excitation of a carbon 1s electron into the mixed  $2\pi/1\pi^*$  molecular orbital characteristic of the pericyclic minimum. The time trace at 284.5 eV shows an instantaneous rise, within the temporal resolution of the experiment, and a decay with a 60 fs time constant, corresponding to the transition from bright to dark state through the first CI; the time trace at 282.2 eV shows a delayed rise (60 fs time constant) and a fast decay (110 fs time constant) characteristic of the intermediate state; finally, the signal at 284.2 eV, rises with 180-fs time constant and is long-lived, signifying the formation of the HT photoproduct. XUV probing of this reaction thus allows one to identify the formation and subsequent decay of the elusive pericyclic minimum, with strong overlap and mixing of the molecular orbitals of the reactant and product. This confirms the Woodward-Hoffmann description of the reaction which assumes a continuous transition of the highest-occupied frontier orbital of the reactant into that of the product.



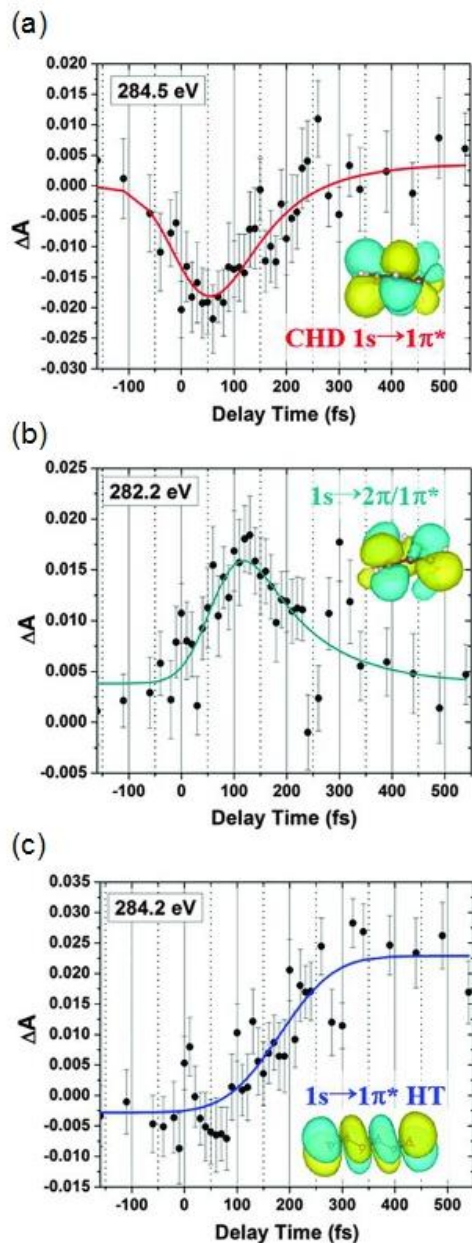


Figure 3.  $\Delta A$  dynamics of CHD at three different probe photon energies: 284.5 eV (a), which is the peak of the carbon  $1s \rightarrow 1\pi^*$  of the reactant; 282.2 eV (b), corresponding to the excitation of a carbon  $1s$  electron into the mixed  $2\pi/1\pi^*$  molecular orbital characteristic of the pericyclic minimum; 284.2 eV, corresponding to the  $1s \rightarrow 1\pi^*$  transition of the ring-opened HT photoproduct. Continuous lines are fits to a convolution of the Gaussian instrumental response function with exponential decay and build-up functions. Figure adapted from Ref. (49).

The second example highlights the novel capabilities offered by attosecond pulses. While femtosecond pulses are perfectly adequate to visualize the atomic motions during a photo-physical/photochemical reaction, the electronic dynamics following the sudden excitation or removal of an electron from a molecule occur on even faster timescales and call for the attosecond temporal resolution. Calegari and coworkers<sup>(52)</sup> performed pump-probe spectroscopy on the aromatic  $\alpha$ -amino acid phenylalanine in the gas phase (Figure 4a). The sample was

excited by a 300-as XUV pulse, generated by HHG and covering the 15–35 eV energy range, and probed by a delayed 4-fs visible pulse at 1.6 eV. The attosecond pump pulse promptly ionizes the molecule and the probe pulse ejects a second electron, producing the immonium di-cation, whose yield is measured by a time-of-flight spectrometer as a function of pump-probe delay. Figure 4b shows the normalized di-cation yield as a function of delay: the signal displays a decay with 25 fs time constant, which is associated to an intramolecular charge transfer process<sup>(53)</sup>. High time resolution measurements (Fig. 4c) clearly show that the di-cation yield dynamics is modulated by an oscillatory pattern, which can be fitted as the superposition of two sine waves with periods of 4.3 fs and 3.4 fs (Figure 4d). The frequency of such oscillations is too high to be due to an impulsively excited molecular vibration, so that they have to be associated to an electronic process. The broadband attosecond XUV pump pulse overlaps with many ionization channels, thus creating a coherent superposition of cationic states which form an electronic wave packet; interaction of this wave packet with the delayed 4-fs probe pulse in turn modulates the di-cation yield.

Numerical simulations of such dynamics, performed within time-dependent density matrix formalism, reproduce the experimental data remarkably well, revealing that the observed oscillations are due to charge dynamics around the amine group. These experiments, made possible by the availability of attosecond pulses, represent the first observation in a biologically relevant molecule of the charge migration dynamics, following instantaneous energy deposition, which precedes nuclear rearrangement. The results are relevant for the understanding of fundamental biological processes such as DNA damage following absorption of an X-ray photon or electron/ion bombardment, or the cellular processes occurring during hadron therapy.

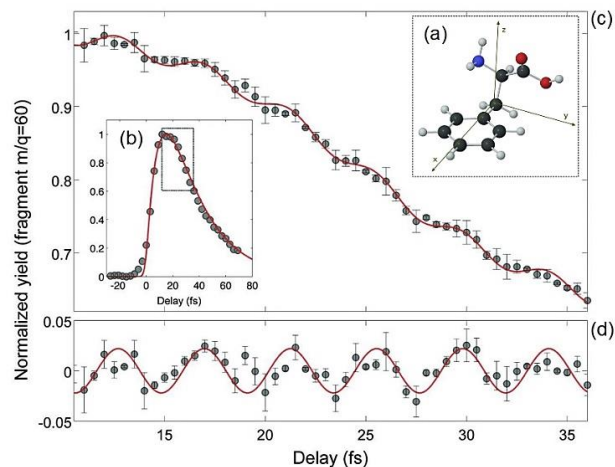


Figure 4. (a) Molecular structure of the most abundant conformer of the aromatic amino acid phenylalanine. (b) Yield of doubly charged immonium ion as a function of pump-probe delay, measured with 3-fs temporal steps. The red line is a fit with exponential build-up of 10 fs and relaxation of 25 fs. (c) Yield of doubly charged immonium ion versus pump-probe delay measured with 0.5-fs temporal steps, within the temporal window shown as dotted box in (b). Error bars show the standard error of the results of four measurements. The red line is the fitting curve given by the sum of the fitting curve shown in (b) and a sinusoidal function of frequency 0.234 PHz (4.3-fs period). (d) Residuals of the data after subtraction of the exponential decay. Red curve is a sinusoidal function of frequency 0.234 PHz. Figure adapted from Ref. (52).

## 2D SPECTROSCOPY

2D spectroscopy allows one to fully measure the third-order nonlinear polarization and thus to extract the maximum amount of information on a system within third-order nonlinear spectroscopy. 2D spectroscopy has delivered a wealth of energetic, dynamical and structural information on (bio)-molecules and nanostructures. It has been used to investigate phenomena spanning from quantum coherence in photosynthesis<sup>(54)-(60)</sup>, to many-body correlations in quantum confined semiconductors<sup>(61), (62)</sup>. 2D spectroscopy has also enabled the identification of specific molecular motions involved in protein folding<sup>(63)-(65)</sup> and structural dynamics<sup>(66)</sup>, as well as chemical reactions and solvation dynamics<sup>(67)-(69)</sup>.

In 2D spectroscopy the system is excited by three distinct time-delayed pulses and the third-order nonlinear signal is recorded in amplitude and phase via the optical heterodyning technique, in which a fourth phase-coherent light pulse, the local oscillator (LO), interferes with the emitted field. By measuring the signal with a spectrometer (which performs a Fourier transform from  $t_3$  to  $\omega_3$ ) and using spectral interferometry<sup>(70)</sup>, one can retrieve the nonlinear signal  $\tilde{P}^{(3)}(t_1, t_2, \omega_3)$ . By performing an additional Fourier transform with respect to  $t_1$  one obtains, for each value of the waiting time  $t_2$ , a 2D map as a function of  $\omega_1$  and  $\omega_3$ ,  $\tilde{P}^{(3)}(\omega_1, t_2, \omega_3)$ . To interpret such maps<sup>(71)</sup>, one can consider  $\omega_1$  as the pump frequency, and  $\omega_3$  as the probe frequency, so that a 2D map corresponds to a collection of TA spectra obtained for different values of the pump frequency  $\omega_1$ . 2D spectroscopy therefore resolves not only in the probe but also in the pump frequency and allows one to identify correlations between excitation and detection frequencies<sup>(72)</sup>.

The diagonal peaks in a 2D map allow to characterize homogeneous and inhomogeneous broadening of transitions and, if recorded as a function of waiting time  $t_2$ , to monitor the loss of excitation memory, also known as spectral diffusion. The cross peaks enable one to identify coupling between different transitions and, if monitored as a function of  $t_2$ , to follow in real time energy relaxation and energy transfer processes. It is important to note that in conventional TA spectroscopy frequency resolution in excitation can only be obtained with narrowband pump pulses, and thus at the expense of temporal resolution; in 2D spectroscopy, on the other hand, thanks to the Fourier transform approach, one can use broadband pump pulses and thus simultaneously maximize time and frequency resolution<sup>(73)</sup>.

2D spectroscopy has a key experimental requirement, which is to maintain phase locking between pulse 1 and pulse 2 (required to perform the Fourier transform with respect to  $t_1$ ) and between pulse 3 and the LO (required to observe their spectral interference). This prerequisite becomes progressively more challenging when moving from the mid-infrared to the visible and the ultraviolet ranges, where a precision of few nanometers is required. For this technical reason, 2D spectroscopy was first developed in the infrared (2DIR spectroscopy<sup>(74)</sup>), targeting vibrational transitions, and only in the last decade it has been extended to the visible (2D electronic spectroscopy, 2DES<sup>(75)</sup>). The extension of 2D spectroscopy to the UV range (2DUV spectroscopy) is still in progress (see Open Challenges section). Two experimental configurations are used to perform 2D spectroscopy, each with advantages and drawbacks: the heterodyne detected three-pulse photon echo<sup>(76)-(78)</sup> and the partially collinear pump-probe geometry<sup>(79)-(81)</sup>. An excellent review of the different experimental configurations, with their advantages and

drawbacks, can be found in Ref. (82). In the following, we present two examples highlighting the power of 2D spectroscopy.

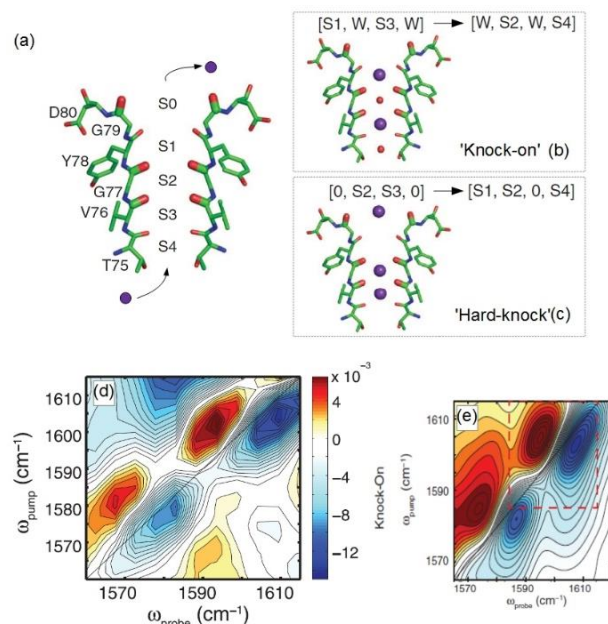


Figure 5. 2DIR spectroscopy reveals the mechanism of  $K^+$  ion permeation in the KscA protein. (a) Scheme of the selectivity filter highlighting the carbonyl groups (oxygen in red) of four amino acids (Thr<sup>75</sup>, Val<sup>76</sup>, Gly<sup>77</sup>, and Tyr<sup>78</sup>) and the binding sites (S1 to S4). (b,c) Schemes of the knock-on (b) and hard-knock (c)  $K^+$  ion permeation mechanisms with the  $K^+$  ions (purple) and the water molecules (red). (d) Experimental 2DIR map obtained by subtraction of the unlabeled spectrum from the labeled spectrum. (e) Simulated 2DIR map for the case of the knock-on mechanism. Figure adapted from Ref. (86).

The first example shows how 2DIR, combined with synthesis of labelled proteins, allows to identify the mechanism of ion permeation within the prototypical transmembrane bacterial channel protein KcsA<sup>(83)</sup>. This protein controls  $K^+$  ion permeation across the cell membrane, which occurs through the so-called selectivity filter, a highly conserved structural element consisting of a narrow pore lined by four backbone carbonyls (S1 to S4 in Figure 5a, labeled from extracellular to intracellular) acting as  $K^+$  binding sites. The mechanism of ion permeation through the selectivity filter in KcsA has been investigated using a variety of experimental and computational approaches<sup>(83)-(85)</sup>.

These studies have proposed two different ion permeation mechanisms. In the first one, referred to as “knock-on” (Figure 5b), the channel is occupied by two  $K^+$  ions (either on S1 and S3 or on S2 and S4 sites) separated by a water molecule; the approach of a third intracellular  $K^+$  ion results in translocation of both a  $K^+$  ion and a water molecule across the membrane. The second mechanism, called “hard-knock” (Figure 5c), postulates that two  $K^+$  ions occupy adjacent binding sites (S2 and S3) in the channel and that translocation occurs through direct collision with a third  $K^+$  ion.

Zanni and coworkers<sup>(86)</sup> have used 2DIR spectroscopy combined with isotope labelling of the ion-binding sites to test the two permeation models. Since molecular vibrations are sensitive to an external electric field, their frequencies depend on the configuration of ions and water molecules within the channel. 2DIR experiments were conducted in KscA proteins with isotopic labelling of the backbone carbonyl groups of the Val<sup>76</sup>,



Gly<sup>77</sup> and Gly<sup>79</sup> residues, which probe the S1, S2 and S3 binding sites. By subtracting the 2DIR maps of labelled and unlabelled proteins, one obtains the differential map reported in Figure 5d, which shows the characteristic features of two well-separated vibrational peaks. The experiments are accurately reproduced by molecular dynamics simulations (Figure 5e) assuming the two K<sup>+</sup> ions at the binding sites separated by a water molecule, thus supporting the knock-on mechanism and ruling out the hard-knock one, which would predict a 2DIR map with only one set of peaks instead of two. This study demonstrates the key contribution that 2DIR spectroscopy can offer to the investigation of dynamics and functional mechanisms in proteins.

The second example demonstrates the capability of 2DES to address the hotly debated question of the presence and the role of excitonic coherences in natural light-harvesting systems. Pioneering 2DES experiments on the photosynthetic Fenna–Matthews–Olson (FMO) complex, a model system for photosynthetic light harvesting<sup>(87)</sup>, revealed long-lived (>1 ps) oscillations of the cross-peaks as a function of waiting time  $t_2$ , first at cryogenic<sup>(54)</sup> and then at physiological temperatures<sup>(57)</sup>. Such oscillations, later observed in antenna complexes of marine algae<sup>(56)</sup> as well as in the light-harvesting antennas<sup>(55)</sup> and the reaction centers<sup>(58),(59)</sup> of higher plants, were assigned to electronic coherences, i.e. coherent superpositions of excitonic states of the complex.

Such coherences were found to be surprisingly long-lived, given the expected short electronic dephasing times caused by interaction of the chromophores with the environment. To explain this observation, the existence of mechanisms protecting electronic coherences in natural light-harvesting systems<sup>(88)</sup> through correlated motions within the protein matrix encapsulating the chromophore was postulated. This has led to the proposition of a new model in which energy transfer in a photosynthetic complex is described by a coherent wavelike motion rather than incoherent hopping.

To investigate this issue, Thyraugh and coworkers applied polarization-controlled 2DES to revisit the coherent dynamics of the FMO complex<sup>(89)</sup>. Figures 6a and 6b show 2DES maps for the all-parallel (AP) and double-crossed (DC) polarization configurations. While the AP map is dominated by diagonal signals corresponding to the excitonic transitions, the DC map displays cross peaks, which reveal correlations between the transitions and shows pronounced oscillations as a function of waiting time  $t_2$ . A detailed analysis of the cross peak dynamics (Figures 6c and 6d), combined with theoretical modelling, enables one to clearly distinguish short-lived excitonic coherences and long-lived vibrational coherences both in the ground and excited states.

The results show that the long-lived oscillations are vibrational in origin, whereas the dephasing of the electronic coherences happens within 240 fs. These data are consistent with a recent room-temperature 2DES study on FMO<sup>(90)</sup>, showing that excitonic coherences dephase on the 60-fs timescale, and point to a negligible role of excitonic coherences in the energy transfer processes in FMO. In general, these results indicate the capability of

2DES to disentangle electronic and vibrational coherences within complex multichromophoric systems, such as those found in photosynthetic complexes.

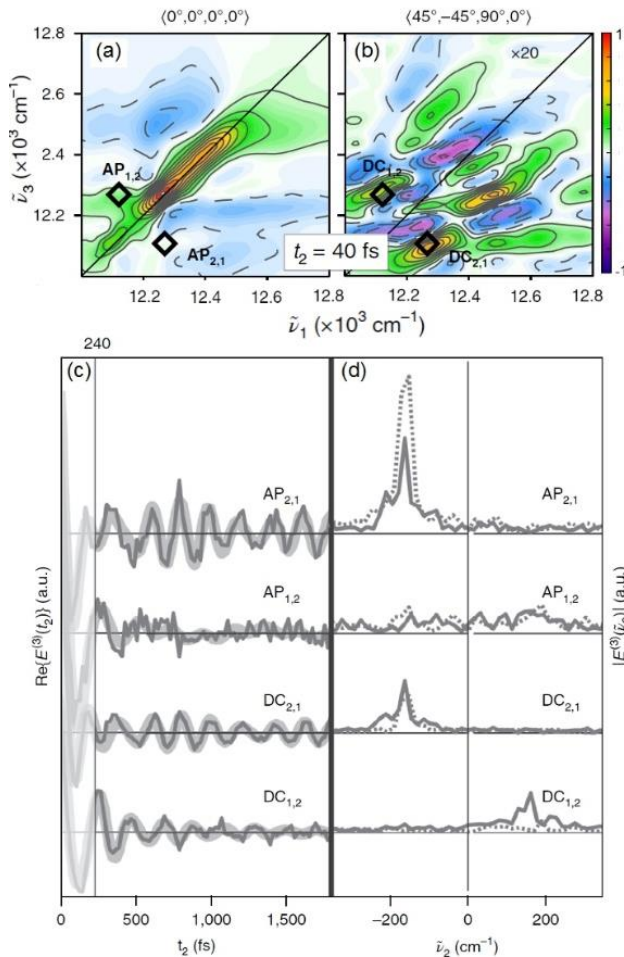


Figure 6. (a, b): 2DES maps for the FMO complex for two different polarization conditions: all-parallel (AP, 0°, 0°, 0°, 0°) (a) and double-crossed (DC, 45°, -45°, 90°, 0°) (b). (c): measured real-part rephasing time traces (thin lines) at the cross-peak locations labelled in (a,b) after subtraction of multi-exponential dynamics; time-domain fits (thick lines) are overlaid onto each trace. (d): Fourier transform amplitudes of the experimental data shown in (c) and the theoretical model data extracted at the same points (broken lines). Figure adapted from Ref. (89).

## ULTRAFAST STRUCTURAL DYNAMICS

Pump-probe and 2D spectroscopy provide information on electronic and nuclear dynamics down to the shortest time scales, however they do not directly measure the structural changes of a molecule or a solid in the course of a photoinduced process, which can in some cases only be inferred from a comparison with numerical simulations. Light (or electron) diffraction has the capability to provide such structural information, by retrieving the time-dependent atomic configuration in real space. However, considering the typical interatomic distances of the order of 1 Å, the diffracted wave should have a comparable wavelength, calling for the use of hard X-rays or energetic (tens of keV) electrons. Femtosecond X-ray and electron diffraction techniques provide the structural sensitivity which allows one to capture the time-dependent evolution of the molecular structure during a light-triggered process, thus fulfilling the

ultimate chemist's dream to shoot a "molecular motion picture" of a photochemical process, watching molecular evolution in space and time. Thanks to the advances in ultrashort X-ray/electron pulse generation, time-resolved diffraction has experienced a great progress in the last decade.

Pioneering studies of time-resolved X-ray diffraction (TR-XRD) were performed with incoherent plasma sources. These experiments allowed the observation of the ultrafast laser-induced changes of long-range order<sup>(91),(92)</sup>, the coherent lattice motions<sup>(93)</sup> that lead to non-thermal melting and coherent phonons in semiconductor nanostructures<sup>(94)</sup>. Using improved plasma sources with higher brightness, it recently became possible to monitor powder X-ray diffraction, allowing simultaneous probing of multiple Bragg peaks<sup>(95)</sup>. TR-XRD allows one to derive transient electron density maps, with 100-fs time resolution and 50-pm spatial resolution, providing insight into field-driven electron relocation<sup>(95)-(97)</sup> and on the interplay of electronic and lattice motion in ionic crystals<sup>(98)</sup>.

The first TR-XRD experiments on protein crystals have been performed at synchrotrons with nanosecond<sup>(99)</sup> to picosecond<sup>(100)</sup> time resolution. Schotte and coworkers studied crystals of carboxy-myoglobin (MbCO). Following CO photolysis with a visible pulse, transient Laue diffraction allowed deriving difference electron density (DED) maps, which unveiled the structural changes on the 100-ps timescale. The results highlighted transient correlated displacements of the heme, the protein backbone and the side chains, which are much larger than the stationary structural changes between the carboxy and deoxy states of Mb, suggesting the possibility that these motions may transiently open a pathway for the ligand to exit from the protein binding site.

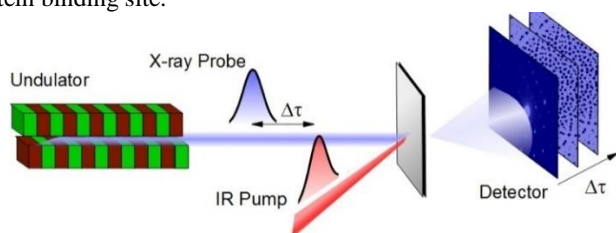


Figure 7. Schematic setup of ultrafast X-ray diffraction using an XFEL. An ultrafast visible pump pulse initiates a photoinduced process in the sample and a time-delayed X-ray probe records a sequence of diffraction patterns as a function of delay  $\Delta t$ .

The shortest pulses that can be produced by synchrotrons have duration of tens of picoseconds; a drastic improvement of the time resolution was possible by XFELs, in particular by the Linac Coherent Light Source (LCLS), which provided access to structural dynamics on the femtosecond timescale. A schematic of an experimental setup for TR-XRD using an XFEL is shown in Figure 7. Barends and coworkers<sup>(101)</sup> extended TR-XRD on MbCO microcrystals to the sub-picosecond timescale. They observed how the CO ligand, within the  $\approx 250$ -fs time resolution of the experiment, moves by 1.6 Å to its transient docking site, located above the heme ring while, at the same time, the heme starts its doming motion and the iron moves out of plane. Vibrational modes of the heme, impulsively excited upon CO photolysis, couple to lower frequency vibrations and ultimately to large scale motions of the protein, leading to displacements of the helices in what had been called a "protein quake"<sup>(102)</sup>. Femtosecond TR-XRD can thus shed new light into the structural evolution following a biochemical process, such as e.g.

ligand dissociation, and to link these dynamics to the biological functions of the protein.

While myoglobin does not utilize light in its natural operation, other proteins are designed to respond to the optical stimulus, such as e.g. in photosynthesis, vision or phototaxis<sup>(103)</sup>. Pande and coworkers<sup>(104)</sup> used XFELs to study the *trans* to *cis* isomerization of the p-coumaric acid (pCA) chromophore in the photoactive yellow protein (PYP), a blue-light sensing protein involved in bacterial phototaxis<sup>(105)</sup>. Photoexcited pCA evolves on the excited *trans* state PES until it reaches a CI, which acts as a gateway from which the wavepacket either relaxes to the final *cis* photoproduct or returns to the ground state of the *trans* reactant<sup>(106)</sup>. The pCA isomerization was initiated by a visible pulse (450-nm wavelength, 140-fs duration) and the structure of PYP was probed by a 40-fs XFEL pulse at 9 keV (1.6 Å). To compensate for the jitter between visible and XFEL pulses, their delay was measured independently with a timing tool<sup>(107)</sup>, thus putting a "time stamp" on each recorded diffraction pattern.

Femtosecond TR-XRD allowed one to make a movie of the structural changes of both the pCA chromophore and the surrounding protein during the early stages of isomerization, which is completed in  $\approx 3$  ps. Early time structural snapshots, derived from the DED maps, retrieve the highly strained *trans* configuration of the chromophore, primed for a transition to *cis*; after 700 fs, the chromophore is already in a *cis* configuration, and the final structure is reached within 3 ps. Global conformational changes of the protein were found to be quite modest, with the average radius increasing by only 0.2% in the first picoseconds. This shows that the protein pocket provides a tight constraint on the chromophore isomerization, which occurs in a volume-conserving fashion. Very recently, TR-XRD has been extended to microcrystals of the retinal-binding-protein bacteriorhodopsin (bR), which acts as a light-driven proton pump, in order to follow, with nearly atomic spatial resolution, the sub-ps *trans-cis* isomerization of the retinal chromophore initiated by a visible pulse<sup>(108)</sup>. The recorded structural dynamics allows one to elucidate the role of the protein pocket in promoting the stereoselectivity and the high quantum yield of the photoisomerization reaction.

Ultrafast electron diffraction (UED) presents different challenges and opportunities with respect to TR-XRD<sup>(34)</sup>. It is now possible to generate bright ultrashort electron pulses containing  $10^5$ – $10^6$  electrons. To avoid multiple scattering effects, samples with thickness of hundreds of nm, similar to those used for transmission electron microscopy, have to be prepared. Pioneering UED experiments have been performed on solids, looking at strongly non-equilibrium states induced by absorption of an ultrashort visible pulse. Siwick and coworkers<sup>(32)</sup> used UED to provide an atomic-level description of the ultrafast melting of aluminum, following in the time domain the loss of the long-range order characteristic of the solid phase. They observed the onset of the liquid structure, with only short-range atomic correlations, within 3 ps, which corresponds to the timescale of thermalization between the photoexcited hot electrons and the cold lattice. The studies were then extended to strongly correlated materials, such as those displaying a charge-density wave (CDW), in which the conduction electron density is modulated, giving rise to a periodic lattice distortion resulting in a lower-energy equilibrium state. UED of the quasi-2D CDW system 1T-TaS<sub>2</sub><sup>(109)</sup> provided an atomic level view of the CDW melting dynamics, allowing one to observe a nearly instantaneous electronically driven cooperative atomic motion resulting in the

suppression of the periodic lattice distortion, followed by thermal disordering due to electron-phonon equilibration.

## OPEN CHALLENGES

The last decade has witnessed a remarkable progress in ultrafast optical spectroscopy, enabled both by technological developments in the generation of ultrashort light/electron pulses and by the introduction of novel spectroscopic techniques. In spite of the many successes, there are still several outstanding challenges, both instrumental and conceptual, which we try to briefly outline in this concluding paragraph.

Transient absorption spectroscopy is a mature technique, with high sensitivity, broad spectral coverage and a very high temporal resolution, approaching the fundamental limit set by the period of the light wave (from a few femtoseconds in the visible down to attoseconds in the XUV). Traditional pump-probe experiments perform averages over a large number of molecules/nanostructures, of the order of  $10^{10}$ - $10^{14}$  in a typical focal volume with 100- $\mu\text{m}$  diameter. The implicit assumption of such ensemble experiments is that all the nano-objects interrogated are identical and evolve in the same fashion. For many systems this is not the case, since the nano-objects, even if nominally identical, present a distribution of internal (conformation, size, shape, ...) as well as external (environment, interface with other nano-objects...) characteristics. This heterogeneity manifests itself not only between different components of an ensemble, but also in a single nano-object, which displays temporal fluctuations of its optical properties due to, e.g., transitions between different conformations.

The limitations of ensemble measurements can be overcome by single-molecule spectroscopy (SMS), a class of techniques which study samples that are sufficiently dilute that only a single nano-object is present in the illuminating light focus. SMS techniques are well established, detecting the fluorescence<sup>(110)</sup> and more recently also the absorption<sup>(111),(112)</sup> of single molecules. Combining TA with SMS is technically challenging, because light focusing is intrinsically limited by diffraction to a diameter of 200-300 nm in the visible, which is 1-2 orders of magnitude larger than the size of a nano-object. There is therefore a large mismatch between the absorption cross section of a single nano-object ( $\sigma_{\text{abs}} = 10^{-16}$ - $10^{-14}$  cm<sup>2</sup>) and the minimum illuminated area in an optical microscope ( $S = 10^{-9}$  cm<sup>2</sup>) so that the absorption signal to be detected is a tiny fraction of the illuminating light background. Pioneering TA experiments on single nano-objects with large absorption cross section (such as metal nanoparticles) have been performed<sup>(113),(114)</sup>, while experiments on single molecules, so far, have exploited detection of fluorescence<sup>(115),(116)</sup>. Improving the sensitivity and exploiting signal enhancement techniques to enable performing TA spectroscopy on single molecules, thus merging the fields of time-resolved and single-molecule spectroscopy, is a promising direction for the future.

2D spectroscopy is nowadays a mature technique in the infrared and visible ranges. The frontier is to broaden the accessible range of measurable frequency correlations, also exploiting two-color methods or the use of continuum probe pulses<sup>(117)</sup>. Current efforts are directed at: (i) extending the spectral range toward the THz and the UV domains; (ii) implementing new type of 2D action spectroscopies (for example 2D electronic spectroscopy in gas phase<sup>(118),(119)</sup>); (iii) developing spatially-re-

solved 2D-fluorescence methods<sup>(120)</sup> with the final goal of obtaining 2D spectra of a single molecule. We will briefly comment on developments in 2D THz and 2D UV spectroscopies.

Recent advances in pulsed, high-power THz sources with electric fields exceeding 100 kV/cm have enabled a new generation of nonlinear THz spectroscopies, in which THz radiation is used to both manipulate and record the response of matter<sup>(121)</sup>. This has allowed extension of 2D spectroscopy to the THz domain using a collinear geometry and field-resolved detection of the nonlinear polarization<sup>(122)</sup>. Experiments are performed with either two or three phase-locked THz pulses. In all cases, amplitude and phase of the transmitted field are measured by electro-optic sampling obtaining, after background subtraction, the nonlinear signal and, after a 2D Fourier transform, the frequency-domain signal. 2D THz spectroscopy has allowed the study of the interaction between inter-subband transitions and optical phonons in semiconductor quantum wells<sup>(123)</sup>, the dynamics of two-phonon coherences in a bulk semiconductor<sup>(124)</sup> and the nonlinear response of collective spin waves in antiferromagnetic crystals<sup>(125)</sup>. So far, the low transition dipoles of low-frequency transitions have prevented the application of 2D THz spectroscopy to pure liquids and biomolecular systems; future work should aim at overcoming this limitation by the use of THz pulses with higher energy.

2DUV spectroscopy is a powerful investigation tool for the structure and dynamics of biomolecules, allowing one for example to study ultrafast photoprotection mechanisms in DNA<sup>(126),(127)</sup> and discriminate the secondary structure of proteins<sup>(128),(129)</sup>. Despite the promising applications, 2DUV spectroscopy has not yet become a mainstream technique due to the significant technical challenges in the generation and characterization of ultrashort UV pulses, as well to the difficulty in achieving phase locking between pulse pairs at short wavelengths. While preliminary promising demonstrations of 2DUV spectroscopy have been performed<sup>(130)-(134)</sup>, mainstream applications of this technique, exploiting its full power to study key biochemical processes, are still lacking. Even more challenging is the extension of 2D spectroscopy to the X-ray domain which, according to calculations by Mukamel and coworkers<sup>(135)</sup>, could directly probe non-Born-Oppenheimer dynamics during CIs<sup>(136)</sup>.

Studies of ultrafast structural dynamics have experienced tremendous progress in recent years, thanks to the development of reliable sources of ultrashort X-ray and electron pulses. Further advances are related to improvement of the source parameters. For XFELs, the highly successful LCLS had a comparatively modest repetition rate of 120 Hz; in the new planned development of LCLS-II the repetition rate will be upgraded to 1 MHz, greatly enhancing the sensitivity and enabling previously impossible experiments. LCLS-II will also feature tunability to the soft X-ray region (200-1000 eV), which is critical for chemistry and materials science. Analogous developments are planned at the European XFEL in Hamburg.

Similar efforts are devoted to improving the flux of femtosecond X-ray incoherent plasma sources. Theoretical simulations, confirmed by experimental results<sup>(137)</sup>, show that the X-ray flux greatly increases by shifting the driving wavelength to the mid-IR, around 5  $\mu\text{m}$ . The recently developed source of energetic ( $\approx 1$  mJ) pulses at 5  $\mu\text{m}$  and 1 kHz repetition rate<sup>(138)</sup> promises to be an ideal driver for high flux table-top femtosecond X-rays, making this technology more broadly available.

In addition to ultrafast electron diffraction, another very promising development is ultrafast electron microscopy

(UEM)<sup>(139)</sup>, in which an optical pump pulse excites the sample that is subsequently probed by an electron pulse in an electron microscope (EM) configuration, either scanning (USEM) or in transmission (UTEM). UEM combines the temporal resolution of ultrafast technique with the spatial resolution of EM, enabling to observe structural dynamics in real time and real space<sup>(140)-(142)</sup>.

In summary, ultrafast optical spectroscopy combines continuous technological advances with conceptual breakthroughs, which broaden its application potential. While the former make it a routine but powerful tool for the investigation of the transient properties of molecules, nanostructures and solids, more and more advanced and previously unthinkable experiments have nowadays become possible. The ultimate chemist's dream of watching the movie of a molecular transformation in time and space is now closer than ever.

## AUTHOR INFORMATION

### Corresponding Author

\* giulio.cerullo@polimi.it

### Author Contributions

The manuscript was written through contributions of all authors

## ACKNOWLEDGMENT

Margherita Maiuri acknowledges support by the Balzan Foundation for the project Q-EX.

## REFERENCES

- (1) Edgerton, H. E.; Killian, J. R. *Moments of Vision - the Stroboscopic Revolution in Photography*; MIT Press, 1979.
- (2) Abraham, H.; Lemoine, T. *Compt. Rend.* **1899**, *129*, 206.
- (3) Norrish, R. G. W.; Porter, G. *Nature* **1949**, *164*, 658.
- (4) Zewail, A. H. *J. Phys. Chem. A* **2000**, *104*, 5660-5694.
- (5) Krausz, F.; Ivanov, M. *Rev. Mod. Phys.* **2009**, *81*, 163-234.
- (6) Elsaesser, T.; *Chem. Rev.* **2017**, *117*, 10621-10622.
- (7) Keller, U. *Nature* **2003**, *424*, 831-838.
- (8) Strickland, D.; Mourou, G. *Opt. Comm.* **1985**, *56*, 219-221.
- (9) Backus, S.; Durfee, C. G.; Murnane, M. M.; Kapteyn, H. C. *Rev. Sci. Instrum.* **1998**, *69*, 1207-23.
- (10) Limpert, J.; Roser, F.; Schreiber, T.; Tunnermann, A. *IEEE J. Sel. Top. Quantum Electron.* **2006**, *12*, 233-244.
- (11) Nisoli, M.; De Silvestri, S.; Svelto, O.; Szpocs, R.; Ferencz, K.; Spielmann, C.; Sartania, S.; Krausz, F. *Opt. Lett.*, **1997**, *22*, 522-524.
- (12) Bradler, M.; Baum, P.; Riedle, E. *Appl. Phys. B* **2009**, *97*, 561.
- (13) Manzoni, C.; Cerullo, G. *J. Opt.* **2016**, *18*, 103501.
- (14) Brida, D.; Manzoni, C.; Cirmi, G.; Marangoni, M.; Bonora, S.; Villorosi, P.; De Silvestri, S.; Cerullo, G. *J. Opt.* **2010**, *12*, 013001.
- (15) Kaindl, R.A.; Wurm, M.; Reimann, K.; Hamm, P.; Weiner, A.M. Woerner, M. *J. Opt. Soc. Am. B* **2000**, *17*, 2086-2094.
- (16) Hoffmann, M.C. and Fülöp, J.A. *J. Phys. D: Appl. Phys.* **2011**, *44*, 083001.
- (17) Megerle, U.; Pugliesi, I.; Schrieffer, C.; Sailer, C. F.; Riedle, E. *Appl. Phys. B* **2009**, *96*, 215-231.
- (18) Trebino, R.; DeLong, K. W.; Fittinghoff, D. N.; Sweetser, J. N.; Krumbügel, M. A.; Richman, B. A.; Kane, D. J. *Rev. Sci. Instrum.* **1997**, *68*, 3277-3295.
- (19) Corkum, P. B. *Phys. Rev. Lett.* **1993**, *71*, 1994-97.
- (20) Sansone, G.; Poletto, L.; Nisoli, M. *Nat. Photonics* **2011**, *5*, 655-663.
- (21) Li, J.; Ren, X.; Yin, Y.; Zhao, K.; Chew, A.; Cheng, Y.; Cunningham, E.; Wang, Y.; Hu, S.; Wu, Y.; Chini, M.; Chang, Z. *Nat. Commun.* **2017**, *8*, 186.
- (22) Schoenlein, R.; Elsaesser, T.; Holldack, K.; Huang, Z.; Kapteyn, H.; Murnane, M.; Woerner, M. *Phil. Trans. R. Soc. A* **2019**, *377*, 20180384.
- (23) Murnane, M.M.; Kapteyn, H.C.; Rosen, M.D.; Falcone, R.W. *Science* **1991**, *251*, 531-536.
- (24) Korn, G.; Thoss, A.; Stiel, H.; Vogt, U.; Richardson, M.; Elsaesser, T.; Faubel, M. *Opt. Lett.* **2002**, *27*, 866-868.
- (25) Zhavoronkov, N.; Gritsai, Y.; Bargheer, M.; Woerner, M.; Elsaesser, T.; Zamponi, F.; Uschmann, I.; Förster, E. *Opt. Lett.* **2005**, *30*, 1737-1739.
- (26) McNeil, B. W. J.; Thompson, N. R. *Nat. Photonics* **2010**, *4*, 814-821.
- (27) Bonifacio, R.; Pellegrini, C.; Narducci, L.M. *Opt. Commun.* **1984**, *50*, 373-378.
- (28) Young, L. et al. *Nature* **2010**, *466*, 56-61.
- (29) Kraus, P. M.; Zürich, M.; Cushing, S. K.; Neumark, D. M.; Leone, S. R. *Nat. Rev. Chem.* **2018**, *2*, 82-94.
- (30) Zholents, A.A.; Zolotarev, M.S. *Phys. Rev. Lett.* **1996**, *76*, 912-915.
- (31) Schoenlein, R.W.; Chattopadhyay, S.; Chong, H.H. W.; Glover, T.E.; Heimann, P.A.; Shank, C.V.; Zholents, A.; Zolotarev, M. *Science* **2000**, *287*, 2237-2240.
- (32) Siwick, B. J.; Dwyer, J. R.; Jordan, R. E.; Miller, R. J. D. *Science* **2003**, *302*, 1382-1385.
- (33) Gao, M.; Jean-Ruel, H.; Cooney, R. R.; Stampe, J.; de Jong, M.; Harb, M.; Sciaini, G.; Moriena, G.; Dwayne Miller, R. J. *Opt. Express* **2012**, *20*, 12048-12058.
- (34) Miller, R. J. D. *Science* **2014**, *343*, 1108-1116.
- (35) Feist, A.; Storeck, G.; Schäfer, S.; Ropers, C. *MRS Bull.* **2018**, *43*, 504-511.
- (36) Mukamel, S. *Principles of Nonlinear Optical Spectroscopy*; Oxford University Press: New York, 1999.
- (37) Schrieffer, C.; Lochbrunner, S.; Riedle, E.; Nesbitt, D. J. *Rev. Sci. Instrum.* **2008**, *79*, 013107.
- (38) Cerullo, G.; Manzoni, C.; Lüer, L.; Polli, D. *Photochem. Photobiol. Sci.* **2007**, *6*, 135-144.
- (39) Polli, D.; Lüer, L.; Cerullo, G. *Rev. Sci. Instrum.* **2007**, *78*, 103108.
- (40) Kovalenko, S.A.; Dobryakov, A.L.; Ruthmann, J.; Ernsting, N.P. *Phys. Rev. A* **1999**, *59*, 2369-2384.
- (41) Polli, D.; Brida, D.; Mukamel, S.; Lanzani, G.; Cerullo, G. *Phys. Rev. A* **2010**, *82*, 053809.



- (42) Polli, D.; Altoè, P.; Weingart, O.; Spillane, K. M.; Manzoni, C.; Brida, D.; Tomasello, G.; Orlandi, G.; Kukura, P.; Mathies, R. A.; Garavelli, M.; Cerullo, G. *Nature* **2010**, *467*, 440-443.
- (43) Ruban, A.V.; Berera, R.; Iliaia, C.; van Stokkum, I.H.M.; Kennis, J.T.M.; Pascal, A.A.; van Amerongen, H.; Robert, B.; Horton, P.; van Grondelle, R. *Nature* **2007**, *450*, 575-578.
- (44) Crespo-Hernández, C.E.; Cohen, B.; Kohler, B. *Nature* **2005**, *436*, 1141-1144.
- (45) Klimov, V.I.; Ivanov, S.A.; Nanda, J.; Achermann, M.; Bezel, I.; McGuire, J.A.; Piryatinski, A. *Nature* **2007**, *447*, 441-446.
- (46) Wu, K.; Chen, J.; McBride, J.R.; Lian, T. *Science* **2015**, *349*, 632-635.
- (47) Günter, G.; Anappara, A.A.; Hees, J.; Sell, A.; Biasiol, G.; Sorba, L.; De Liberato, S.; Ciuti, C.; Tredicucci, A.; Leitenstorfer, A.; Huber, A. *Nature* **2009**, *458*, 178-181.
- (48) Gélinas, S.; Rao, A.; Kumar, A.; Smith, S.L.; Chin, A.W.; Clark, J.; van der Poll, T.S.; Bazan, G.C.; Friend, R.H. *Science* **2014**, *343*, 512-516.
- (49) Attar, A. R.; Bhattacharjee, A.; Pemmaraju, C. D.; Schnorr, K.; Closser, K. D.; Prendergast, D.; Leone, S. R. *Science* **2017**, *356*, 54-59.
- (50) Hoffmann, R.; Woodward, R. B. *Acc. Chem. Res.* **1968**, *1*, 17-22.
- (51) Garavelli, M.; Page, C. S.; Celani, P.; Olivucci, M.; Schmid, W. E.; Trushin, S. A.; Fuss, W. *J. Phys. Chem. A* **2001**, *105*, 4458-4469.
- (52) Calegari, F.; Ayuso, D.; Trabattoni, A.; Belshaw, L.; De Camillis, S.; Anumula, S.; Frassetto, F.; Poletto, L.; Palacios, A.; Decleva, P.; Greenwood, J. B.; Martín, F.; Nisoli, M. *Science* **2014**, *346*, 336-339.
- (53) Belshaw, L.; Calegari, F.; Duffy, M. J.; Trabattoni, A.; Poletto, L.; Nisoli, M.; Greenwood, J. B. *J. Phys. Chem. Lett.* **2012**, *3*, 3751-3754.
- (54) Engel, G.S.; Calhoun, T.R.; Read, E.L.; Ahn, T.-K.; Mancal, T.; Cheng, Y.-C.; Blankenship, R.E.; Fleming, G.R. *Nature* **2007**, *446*, 782-786.
- (55) Calhoun, T.R.; Ginsberg, N.S.; Schlau-Cohen, G.S.; Cheng, Y.-C.; Ballottari, M.; Bassi, R.; Fleming, G.R. *J. Phys. Chem. B*, **2009**, *113*, 16291-16295.
- (56) Collini, E.; Wong, C.Y.; Wilk, K.E.; Curmi, P.M.G.; Brumer, P.; Scholes, G.D. *Nature*, **2010**, *463*, 644-647.
- (57) Panitchayangkoon, G.; Hayes, D.; Fransted, K.A.; Caram, J.R.; Harel, E.; Wen, J.; Blankenship, R.E.; Engel, G.S. *Proc. Natl. Acad. Sci. USA*, **2010**, *107*, 12766-12770.
- (58) Fuller, F.D.; Pan, J.; Gelzini, A.; Butkus, V.; Senlik, S.S.; Wilcox, D.E.; Yocum, C.F.; Valkunas, L.; Abramavicius, D.; Ogilvie, J.P. *Nat. Chem.*, **2014**, *6*, 706-711.
- (59) Romero, E.; Novoderezhkin, V.I.; van Grondelle, R. *Nature*, **2017**, *543*, 355-365.
- (60) Scholes, G.D.; Scholes, G.D.; Fleming, G.R.; Chen, L.X.; Aspuru-Guzik, A.; Buchleitner, A.; Coker, D.F.; Engel, G.S.; van Grondelle, R.; Ishizaki, A.; Jonas, D.M.; Lundeen, J.S.; McCusker, J.K.; Mukamel, S.; Ogilvie, J.P.; Olaya-Castro, A.; Ratner, M.A.; Spano, F.C.; Whaley, K.B.; Zhu, X. *Nature*, **2017**, *543*, 647-656.
- (61) Stone, K.W.; Gundogdu, K.; Turner, D.B.; Li, X.; Cundiff, S.T.; Nelson, K.A. *Science* **2009**, *324*, 1169-1173.
- (62) Moody, G.; Cundiff, S.T. *Adv Phys X* **2017**, *2*, 641-674.
- (63) Chung, H.S.; Ganim, Z.; Jones, K.C.; Tokmakoff, A. *Proc. Natl Acad. Sci. USA*, **2007**, *104*, 14237-14 242.
- (64) Strasfeld, D.B.; Ling, Y.L.; Shim, S.-H.; Zanni, M.T. *J. Am. Chem. Soc.*, **2008**, *130*, 6698-6699.
- (65) Shim, S.-H.; Gupta, R.; Ling, Y.L.; Strasfeld, D.B.; Raleigh, D.P.; Zanni, M.T. *Proc. Natl Acad. Sci. USA*, **2009**, *106*, 6614-6619.
- (66) Ghosh, A.; Qiu, J.; DeGrado, W.F.; Hochstrasser, R.M. *Proc. Natl Acad. Sci. USA*, **2011**, *108*, 6115-6120.
- (67) Ramasesha, K.; De Marco, L.; Mandal, A.; Tokmakoff, A. *Nat. Chem.*, **2013**, *5*, 935-940.
- (68) Ruetzel, S.; Diekmann, M.; Nuernberger, P.; Walter, C.; Engels, B.; Brixner, T. *Proc. Natl Acad. Sci. USA*, **2014**, *111*, 4764-4769.
- (69) Dahms, F.; Fingerhut, B.P.; Nibbering, E.T.J.; Pines, E.; Elsaesser, T. *Science*, **2017**, *357*, 491-495.
- (70) Lepetit, L.; Chériaux, G.; Joffe, M. *J. Opt. Soc. Am. B* **1995**, *12*, 2467-74.
- (71) Hamm, P.; Zanni, M. T. *Concepts and Methods of 2d Infrared Spectroscopy*; Cambridge University Press: Cambridge ; New York, 2011.
- (72) Hochstrasser, R. M. *P. Natl. Acad. Sci. USA* **2007**, *104*, 14190-14196.
- (73) Mukamel, S. *Annu. Rev. Phys. Chem.* **2000**, *51*, 691-729.
- (74) Hamm, P.; Lim, M.; Hochstrasser, R. M. *J. Phys. Chem. B* **1998**, *102*, 6123-6138.
- (75) Brixner, T.; Stenger, J.; Vaswani, H. M.; Cho, M.; Blankenship, R. E.; Fleming, G. R. *Nature* **2005**, *434*, 625-628.
- (76) Cowan, M. L.; Ogilvie, J. P.; Miller, R. J. D. *Chem. Phys. Lett.* **2004**, *386*, 184-189.
- (77) Brixner, T.; Stiopkin, I. V.; Fleming, G. R. *Opt. Lett.* **2004**, *29*, 884-886.
- (78) Nemeth, A.; Sperling, J.; Hauer, J.; Kauffmann, H. F.; Milota, F. *Opt. Lett.* **2009**, *34*, 3301-3303.
- (79) DeFlores, L. P.; Nicodemus, R. A.; Tokmakoff, A. *Opt. Lett.* **2007**, *32*, 2966-2968.
- (80) Shim, S.-H.; Strasfeld, D. B.; Ling, Y. L.; Zanni, M. T. *P. Natl. Acad. Sci. USA* **2007**, *104*, 14197-14202.
- (81) Grumstrup, E. M.; Shim, S.-H.; Montgomery, M. A.; Damrauer, N. H.; Zanni, M. T. *Opt. Express* **2007**, *15*, 16681-16689.
- (82) Fuller, F. D.; Ogilvie, J. P. *Annu. Rev. Phys. Chem.* **2015**, *66*, 667-690.
- (83) Doyle, D. A.; Morais Cabral, J.; Pfuetzner, R.A.; Kuo, A.; Gulbis, J.M.; Cohen, S.L.; Chait, B.T.; MacKinnon, R. *Science* **1998**, *280*, 69-77.
- (84) Morais-Cabral, J.H.; Zhou, Y.; MacKinnon, R. *Nature* **2001**, *414*, 37-42.

- (85) Uysal, S.; Vásquez, V.; Tereshko, V.; Esaki, K.; Fellouse, F.A.; Sidhu, S.S.; Koide, S.; Perozo, E.; Kossiakoff, A. *Proc. Natl. Acad. Sci. U.S.A.* **2009**, *106*, 6644–6649.
- (86) Kratochvil, H.T.; Carr, J.K.; Matulef, K.; Annen, A.W.; Li, H.; Maj, M.; Ostmeyer, J.; Serrano, A.L.; Raghuraman, H.; Moran, S.D.; Skinner, J.L.; Perozo, E.; Roux, B.; Valiyaveetil, F.I.; Zanni, M.T. *Science* **2016**, *353*, 1040–1044.
- (87) Fenna, R.; Matthews, B. *Nature* **1975**, *258*, 573–577.
- (88) Lee, H.; Cheng, Y.-C.; Fleming, G.R. *Science* **2007**, *316*, 1462–1465.
- (89) Thyryhaug, E.; Tempelaar, R.; Alcocer, M. J. P.; Židek, K.; Bina, D.; Knoester, J.; Jansen, T. L. C.; Zigmantas, D. *Nat. Chem.* **2018**, *10*, 780–786.
- (90) Duan, H.-G.; Prokhorenko, V. I.; Cogdell, R. J.; Ashraf, K.; Stevens, A. L.; Thorwart, M.; Miller, R. J. D. *P. Natl. Acad. Sci. USA* **2017**, *114*, 8493–8498.
- (91) Siders, C.W.; Cavalleri, A.; Sokolowski-Tinten, K.; Tóth, Cs.; Guo, T.; Kammler, M.; Horn von Hoegen, M.; Wilson, K.R.; von der Linde, D.; Barty, C.P.J. *Science* **1999**, *286*, 1340–1342.
- (92) Rousse, A.; Rischel, C.; Fourmaux, S.; Uschmann, I.; Sebban, S.; Grillon, G.; Balcou, Ph.; Förster, E.; Geindre, J.P.; Audebert, P.; Gauthier, J.C.; Hulin, D. *Nature* **2001**, *410*, 65–68.
- (93) Sokolowski-Tinten, K.; Blome, C.; Blums, J.; Cavalleri, A.; Dietrich, ; Tarasevitch, A.; Uschmann, I.; Förster, E.; Kammler, M.; Horn-von-Hoegen, M.; von der Linde, D. *Nature* **2003**, *422*, 287–289.
- (94) Bargheer, M.; Zhavoronkov, N.; Gritsai, Y.; Woo, J. C.; Kim, D. S.; Woerner, M.; Elsaesser, T. *Science* **2004**, *306*, 1771–1773.
- (95) Zamponi, F.; Ansari, Z.; Woerner, M.; Elsaesser, T. *Opt. Express* **2010**, *18*, 947–961.
- (96) Stingl, J.; Zamponi, F.; Freyer, B.; Woerner, M.; Elsaesser, T.; Borgschulte, A. *Phys. Rev. Lett.* **2012**, *109*, 147402.
- (97) Juvé, V.; Holtz, M.; Zamponi, F.; Woerner, M.; Elsaesser, T.; Borgschulte, A. *Phys. Rev. Lett.* **2013**, *111*, 217401.
- (98) Zamponi, F.; Rothhardt, P.; Stingl, J.; Woerner, M.; Elsaesser, T. *Proc. Natl. Acad. Sci. U.S.A.* **2012**, *109*, 5207.
- (99) Šrajer, V.; Teng, T.; Ursby, T.; Pradervand, C.; Ren, Z.; Adachi, S.; Schildkamp, W.; Bourgeois, D.; Wulff, M.; Moffat, K. *Science* **1996**, *274*, 1726–1729.
- (100) Schotte, F.; Lim, M.; Jackson, T. A.; Smirnov, A. V.; Soman, J.; Olson, J. S.; Phillips, G. N.; Wulff, M.; Anfinrud, P. A. *Science* **2003**, *300*, 1944–1947.
- (101) Barends, T. R. M. et al. *Science* **2015**, *350*, 445–450.
- (102) Ansari, A.; Berendzen, J.; Bowne, S. F.; Frauenfelder, H.; Iben, I. E.; Sauke, T. B.; Shyamsunder, E.; Young, R. D. *P. Natl. Acad. Sci. USA* **1985**, *82*, 5000–5004.
- (103) Sundström, V. *Annu. Rev. Phys. Chem.* **2008**, *59*, 53–77.
- (104) Pande, K. et al. *Science* **2016**, *352*, 725–729.
- (105) Hellingwerf, K. J.; Hendriks, J.; Gensch, T. *J. Phys. Chem. A* **2003**, *107*, 1082–1094.
- (106) Larsen, D. S.; Vengris, M.; van Stokkum, I. H. M.; van der Horst, M. A.; de Weerd, F. L.; Hellingwerf, K. J.; van Grondelle, R. *Biophys. J.* **2004**, *86*, 2538–2550.
- (107) Harmand, M.; Coffee, R.; Bionta, M. R.; Chollet, M.; French, D.; Zhu, D.; Fritz, D. M.; Lemke, H. T.; Medvedev, N.; Ziaja, B.; Toleikis, S.; Cammarata, M. *Nat. Photonics* **2013**, *7*, 215–218.
- (108) Nogly, P. et al. *Science* **2018**, *361*, eaat0094.
- (109) Eichberger, M.; Schäfer, H.; Krumova, M.; Beyer, M.; Demsar, J.; Berger, H.; Moriena, G.; Sciaini, G.; Miller, R. J. D. *Nature* **2010**, *468*, 799–802.
- (110) Orrit, M.; Bernard, J. *Phys. Rev. Lett.* **1990**, *65*, 2716–2719.
- (111) Gaiduk, A.; Yorulmaz, M.; Ruijgrok, P. V.; Orrit, M. *Science* **2010**, *330*, 353–356.
- (112) Celebrano, M.; Kukura, P.; Renn, A.; Sandoghdar, V. *Nat. Photonics* **2011**, *5*, 95–98.
- (113) Baida, H.; Mongin, D.; Christofilos, D.; Bachelier, G.; Crut, A.; Maioli, P.; Del Fatti, N.; Vallée, F. *Phys. Rev. Lett.* **2011**, *107*, 057402.
- (114) van Dijk, M. A.; Lippitz, M.; Orrit, M. *Phys. Rev. Lett.* **2005**, *95*, 267406.
- (115) Hildner, R.; Brinks, D.; Nieder, J. B.; Cogdell, R. J.; van Hulst, N. F. *Science* **2013**, *340*, 1448–1451.
- (116) Liebel, M.; Toninelli, C.; van Hulst, N. F. *Nat. Photonics* **2018**, *12*, 45–49.
- (117) Song, Y.; Konar, A.; Sechrist, R.; Prakash Roy, V.; Duan, R.; Dziurgot, J.; Policht, V.; Acosta Matutes, Y.; Kubarych, K.J.; Ogilvie, J.P. *Rev. Sci. Instrum.* **2019**, *90*, 013108.
- (118) Roeding, S.; Brixner, T. *Nat. Commun.* **2018**, *9*, 2519.
- (119) Bruder, L.; Bangert, U.; M. Binz, M.; Uhl, D.; Vexiau, R.; Bouloufa-Maafa, N.; Dulieu, O.; Stienkemeier, F. *Nat. Commun.* **2018**, *9*, 4823.
- (120) Tiwari, V.; Acosta Matutes, Y.; Gardiner, A.T.; LC Jansen, T.; Cogdell, R.J.; Ogilvie, J.P. *Nat. Commun.* **2018**, *9*, 4219.
- (121) Kampfrath, T.; Tanaka, K.; Nelson, K.A. *Nat. Photonics* **2013**, *7*, 680–690.
- (122) Woerner, M.; Kuehn, W.; Bowlan, P.; Reimann, K.; Elsaesser, T. *New J. Phys.* **2013**, *15*, 025039.
- (123) Kuehn, W.; Reimann, K.; Woerner, M.; Elsaesser, T.; Hey, R.; Schade, U. *Phys. Rev. Lett.* **2011**, *107*, 067401.
- (124) Somma, C.; Folpini, G.; Reimann, K.; Woerner, M.; Elsaesser, T. *Phys. Rev. Lett.* **2016**, *116*, 177401.
- (125) Lu, J.; Li, X.; Hwang, H.Y.; Ofori-Okai, B.K.; T. Kurihara, T.; Suemoto, T.; Nelson, K.A. *Phys. Rev. Lett.* **2017**, *118*, 207204.
- (126) Middleton, C. T.; Harpe, K. d. L.; Su, C.; Law, Y. K.; Crespo-Hernández, C. E.; Kohler, B. *Annu. Rev. Phys. Chem.* **2009**, *60*, 217–239.
- (127) Li, Q.; Giussani, A.; Segarra-Martí, J.; Nenov, A.; Rivalta, I.; Voityuk, A. A.; Mukamel, S.; Roca-Sanjuán, D.; Garavelli, M.; Blancafort, L. *Chemistry* **2016**, *22*, 7497–7507.
- (128) Jiang, J.; Mukamel, S. *Angew. Chem., Int. ed.* **2010**, *49*, 9666–9669.

- (129) Nenov, A.; Rivalta, I.; Cerullo, G.; Mukamel, S.; Garavelli, M. *J. Phys. Chem. Lett.* **2014**, *5*, 767-771.
- (130) West, B. A.; Womick, J. M.; Moran, A. M. *J. Phys. Chem. A* **2011**, *115*, 8630-8637.
- (131) Tseng, C.-H.; Sándor, P.; Kotur, M.; Weinacht, T. C.; Matsika, S. *J. Phys. Chem. A* **2012**, *116*, 2654-2661.
- (132) Consani, C.; Auböck, G.; van Mourik, F.; Chergui, M. *Science* **2013**, *339*, 1586-1589.
- (133) Krebs, N.; Pugliesi, I.; Hauer, J.; Riedle, E. *New J. Phys.* **2013**, *15*, 085016.
- (134) Borrego-Varillas, R.; Oriana, A.; Ganzer, L.; Trifonov, A.; Buchvarov, I.; Manzoni, C.; Cerullo, G. *Opt. Express* **2016**, *24*, 28491-28499.
- (135) Mukamel, S.; Healion, D.; Zhang, Y.; Biggs, J.D. *Annu. Rev. Phys. Chem.* **2013**, *64*, 101-127.
- (136) Kowalewski, M.; Bennett, K.; Dorfman, K.E.; Mukamel, S. *Phys. Rev. Lett.* **2015**, *115*, 19 003-193006.
- (137) Weisshaupt, J.; Juvé, V.; Holtz, M.; Ku, S.; Woerner, M.; Elsaesser, T.; Ališauskas, S.; Pugžlys, A.; Baltuška, A. *Nat. Photonics* **2014**, *8*, 927-930.
- (138) von Grafenstein, L.; Bock, M.; Ueberschaer, D.; Zawilski, K.; Schunemann, P.; Griebner, U.; Elsaesser, T. *Opt. Lett.* **2017**, *42*, 3796-3799.
- (139) Zewail, A. H. *Science* **2010**, *328*, 187-193.
- (140) Baum, P.; Yang, D.-S.; Zewail, A. H. *Science* **2007**, *318*, 788-792.
- (141) van der Veen, R. M.; Kwon, O.-H.; Tissot, A.; Hauser, A.; Zewail, A. H. *Nat. Chem.* **2013**, *5*, 395-402.
- (142) Gulde, M.; Schweda, S.; Storeck, G.; Maiti, M.; Yu, H.K.; Wodtke, A.M.; Schäfer, S.; Ropers, C. *Science* **2014**, *345*, 200-204.

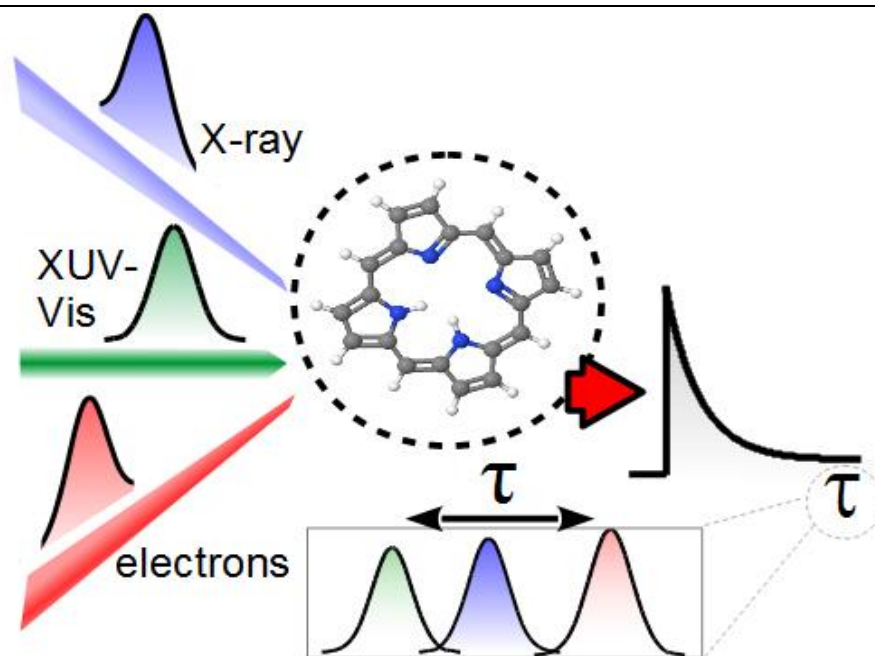


Table of Contents artwork